Accepted Manuscript

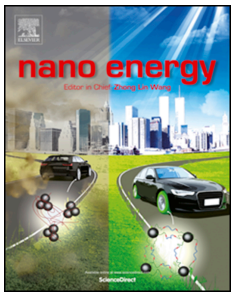

In-situ visualization of lithium plating in all-solid-state lithium-metal battery

Quan Li, Tiancheng Yi, Xuelong Wang, Hongyi Pan, Baogang Quan, Tianjiao Liang, Xiangxin Guo, Xiqian Yu, Howard Wang, Xuejie Huang, Liquan Chen, Hong Li

PII: S2211-2855(19)30602-0

DOI: https://doi.org/10.1016/j.nanoen.2019.103895

Article Number: 103895

Reference: NANOEN 103895

To appear in: *Nano Energy*

Received Date: 31 May 2019

Revised Date: 27 June 2019

Accepted Date: 9 July 2019

Please cite this article as: Q. Li, T. Yi, X. Wang, H. Pan, B. Quan, T. Liang, X. Guo, X. Yu, H. Wang, X. Huang, L. Chen, H. Li, *In-situ* visualization of lithium plating in all-solid-state lithium-metal battery, *Nano Energy* (2019), doi: https://doi.org/10.1016/j.nanoen.2019.103895.

TOC Figure

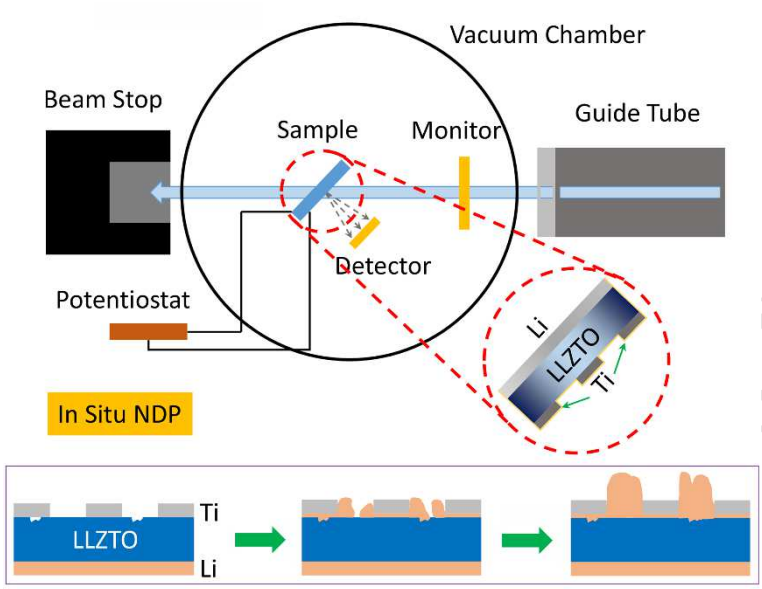

In-situ Visualization of Lithium Plating in All-Solid-State Lithium-Metal Battery

Quan Li[1,2], Tiancheng Yi[3,4], Xuelong Wang[1,2], Hongyi Pan[1,2], Baogang Quan[1], Tianjiao Liang[3,4*], Xiangxin Guo[5], Xiqian Yu[1,2], Howard Wang[6*], Xuejie Huang[1,2], Liquan Chen[1,2], Hong Li[1,2*]

1. Beijing Advanced Innovation Center for Materials Genome Engineering, Institute of Physics, Chinese Academy of Science, Beijing 100190, China
2. Center of Materials Science and Optoelectronics Engineering, University of Chinese Academy of Sciences, Beijing 100049, China
3. Institute of High Energy Physics, Chinese Academy of Science, Beijing 100049, China
4. Dongguan Neutron Science Center, Dongguan 523803, China
5. College of Physics, Qingdao University, Qingdao 266071, China
6. Department of Materials Science and Engineering, University of Maryland, College Park, Maryland 20742, United States

Corresponding Author

*E-mail address: hli@iphy.ac.cn; tjliang@ihep.ac.cn; wangh@umd.edu

Keywords: solid-state battery, lithium metal anode, three dimensional electrode, interface, lithium dendrite

Abstract

Lithium metal with high theoretical specific capacity (3860 mAh/g) and the lowest electrochemical potential (-3.04 V vs standard hydrogen electrode) has been considered as the most promising anode material for next-generation rechargeable batteries. Since lithium readily reacts with most organic solvents, complete replacement of conventional electrolytes with solid electrolyte has attracted much attention. However, in solid-state lithium batteries uncontrollable lithium dendrites growth and large interface fluctuations during lithium plating/stripping still happens, leading to short circuit or capacity fading. This study employs Neutron Depth Profile (NDP), a unique tool with high sensitivity and high spatial resolution for lithium detection in solid device, to investigate the lithium plating behavior in Li|$Li_{6.4}La_3Zr_{1.4}Ta_{0.6}O_{12}$ (LLZTO) |Ti solid-state battery with three-dimensional (3D) Ti electrode. The experiments, together with theoretical modeling, show that the majority of lithium can be deposited in the void space of the Ti 3D electrode which largely diminishes solid electrolyte/electrode interface degradation and suppresses lithium dendrite growth as well. This research demonstrates that a negative electrode with efficiently designed 3D framework can not only undertake the huge volume expansion during lithium plating but also regulate lithium deposition behavior to inhibit Li dendrite growth.

Introduction

Lithium ion batteries (LIBs) have been widely used in portable electronics, electric vehicles and large-scale energy storage systems for their high energy density [1, 2]. At present, the increasing demands for energy put high requirements for energy density on battery systems [3]. However, in traditional LIBs that use non-aqueous liquid electrolyte, it is hard to achieve high energy density and high safety at the same time [4, 5]. Though optimizing the liquid organic electrolyte by adding functional additives does have positive impacts on battery performance, it cannot yet be considered as a perfect solution [6-10]. Replacing liquid electrolyte by solid electrolyte has been considered as an alternative approach to address the critical safety issues [11-14]. Solid electrolyte materials usually possess higher chemical stability and mechanical strength compared to conventional liquid electrolytes. More importantly, using solid electrolyte may also realize the employment of metallic lithium anode, which benefits the increase of energy density [15-19]. However, recent studies indicate that solid electrolyte still cannot solve the notorious lithium dendrite problem thoroughly [20-22], and the mechanism of lithium dendrite growth in solid-state batteries is still under debating [21, 23, 24]. In addition, the swelling [25-28] of lithium metal electrode over the charge-discharge processes will lead to continuous increase of cell resistances due to the degradation of the solid electrolyte and electrode interface [29-34]. Therefore, the interface and dendrites issues are the major roadblocks for the practical applications of the solid-state lithium batteries [35-38]. Design of electrodes with three-dimensional (3D) framework has proven to be an effective strategy to

overcome the dendrite growth problem in LIBs with liquid electrolyte [39-44]. Not only it can regulate lithium plating behavior to avoid the dendrite growth, but also it can accommodate lithium storage and moderate volume expansion. It is therefore necessary to study the lithium plating/stripping behavior in solid-state batteries with 3D electrode. Unfortunately, only scattered studies have been devoted to this research area, very likely due to shortage of effective, non-destructive characterizing methods for direct observation of lithium deposition process in solid-state batteries.

In the present work, the lithium dendrites growth and crack propagation in Li|$Li_{6.4}La_3Zr_{1.4}Ta_{0.6}O_{12}$ (LLZTO)|Li solid-state battery are observed for the first time by employing an self-designed *in-situ* probing station that can be installed in the Scanning Electron Microscope. The lithium plating/striping behavior at the interface between intimately contacted solid electrolyte and flat Li electrode has been studied. Furthermore, an all-solid-state lithium metal battery (ASSLMB) with 3D Ti (w/ 3D Ti) electrode adhering to the flat garnet electrolyte LLZTO pellet and lithium metal as the counter electrode was constructed. *In-situ* Neutron Depth Profile (NDP) [24, 45-49], a unique non-destructive characterizing technique with high spatial resolution, high detection sensitivity of lithium, was employed to study lithium plating behavior in 3D electrode. The lithium storage in the void space of the 3D electrode was directly visualized and the ignorable dendrite growth was further confirmed by *ex-situ* SEM measurements. For comparison, an all-solid-state lithium metal battery (ASSLMB) without 3D Ti (w/o 3D Ti) electrode was also investigated, in which we observed lithium metal broke Ti film and lithium dendrites grow uncontrollably.

Results

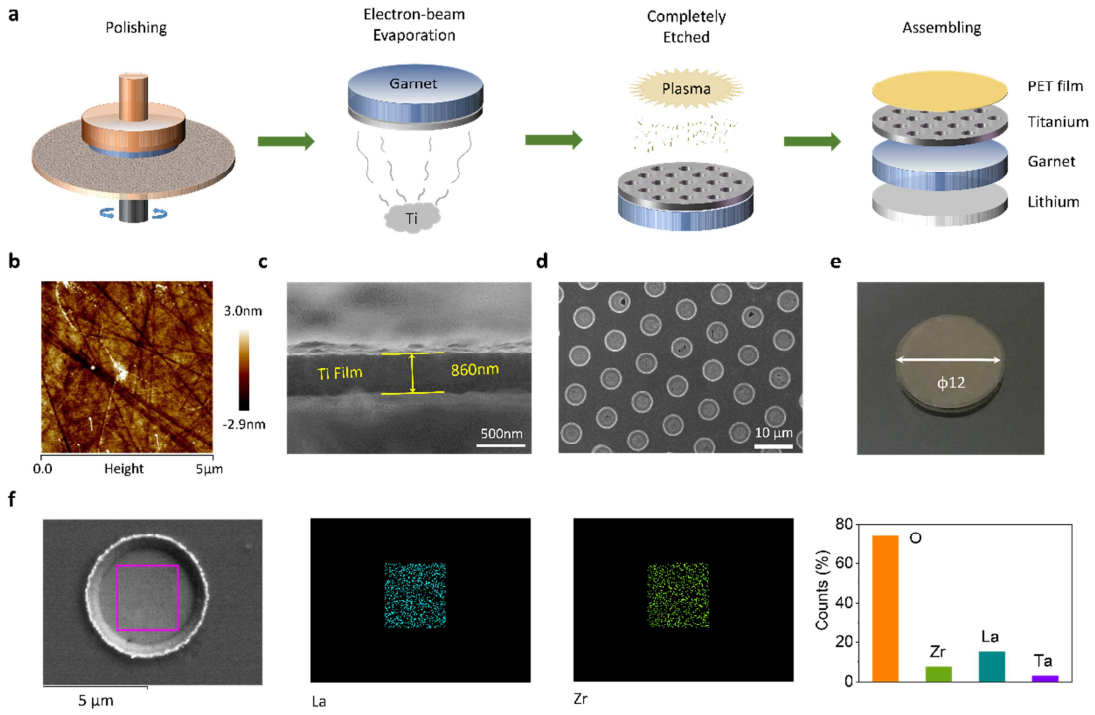

Fig. 1 Fabrication of all solid-state lithium metal battery with 3D Ti (ASSLMB w/ 3D Ti) electrode. (a) Schematic illustrations of the key procedures for constructing the ASSLMB w/ 3D Ti electrode. The corresponding characterizations for each steps are shown as **(b)** surface morphology of the LLZTO pellet after polishing. **(c)** Cross-sectional view of the Ti film fabricated by electron-beam evaporation. **(d)** Patterned Ti electrode obtained after ion-beam etching and **(e)** optical image of the ASSLMB w/ 3D Ti electrode. **(f)** Element mapping performed on the void region. The detection of Zr and Ta indicates that the Ti film is completely etched.

The fabrication of the solid-state battery is followed by a series of micro-fabrication processes as schematically shown in Fig. 1a. First, the super high density garnet

electrolyte $Li_{6.4}La_3Zr_{1.4}Ta_{0.6}O_7$ (LLZTO) pellet (see as Fig. S1) was polished, on which Ti was deposited by electron-beam evaporation. The surface morphology of the LLZTO pellet was probed by atomic force microscope (AFM). After polishing, the surface roughness of the pellet was well controlled to a fluctuation range less than 6 nm (Fig. 1b), to meet the rigorous requirement for the NDP measurement. Then, Ti film was deposited with a thickness of 860 nm (Fig. 1c). It can be found that the pristine Ti film is homogeneous and flat (Fig. S2). After that, a combination of UV exposure and Ar^+ ion beam etching processes was conducted to fabricate patterned Ti electrode (Fig. S3). The designed pattern consists of hexagonal arranged circular holes with a diameter of 5 μm (Fig. 1d and Fig. S4). It is important that the Ti film must be completely etched to expose the LLZTO electrolyte, in order to produce an open void space for lithium plating. After that, the photoresist was etched off with oxygen plasma to get the clean Ti surface. The thickness and surface flatness of the Ti film are not changed with these processes, confirmed by stylus profiler (Fig. S5, Table S1). In order to verify that the Ti film is completely etched, an energy dispersive spectrometer (EDS) measurement was conducted to scan the element distribution in the hole's region. The results shown in Fig. 1f and S6 clearly indicate that Ti film was completely etched as the Ta and Zr elements in LLZTO can be detected. The whole battery was then assembled by pressing the Li foil on LLZTO and sealed the whole part with PET film in a soft pack formation (Fig. 1e). It should be noted there are two copper current collectors stretch out of the soft pack cell at both Ti and Li electrode side.

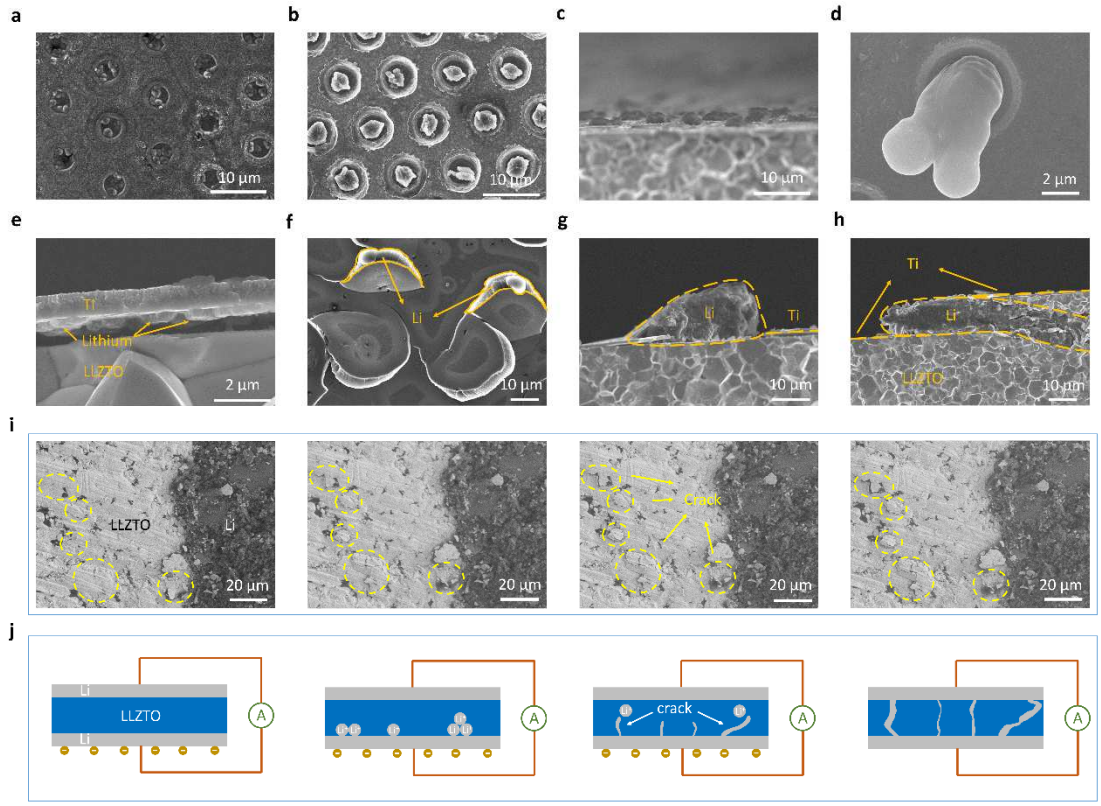

Fig. 2 Morphology of lithium plating. Surface morphology of patterned Ti electrode after lithium plating with **(a)** low capacity (half storable capacity of the holes, 23 μAh/cm^2) and **(b)** high capacity (equal to storable capacity of the holes, 45 μAh/cm^2). **(c)** Cross-sectional view of **b.** **(d)** Enlarged view of surface morphology at a larger capacity of 90 μAh/cm^2. **(e)** Cross-sectional view of ASSLMB w/o 3D Ti electrode after lithium plating (23 μAh/cm^2). **(f)** Surface morphology of ASSLMB w/o 3D Ti electrode after lithium plating (90 μAh/cm^2). **(g)** and **(h)** Cross-sectional view of short-circuited ASSLMB at the Ti film side. **(i)** *In-situ* cross-sectional morphology evolution of LLZTO in Li|LLZTO|Li solid-state symmetric battery. **(j)** The schematic illustration of **i**.

SEM measurements were performed to study the lithium plating behavior in

ASSLMB w/ 3D Ti electrode. The lithium plating process was controlled by discharging the solid-state batteries to different capacities. The lithium firstly deposited along the wall of the holes where electronic conducting was favorable with a low capacity of half storable capacity of the holes, 23 μAh/cm^2 (Fig. 2a). Then lithium would accumulate and tend to fill the holes with 2 times discharge capacity increasing (Fig. 2b, 2c) where no obvious dendrite growth can be observed. In the condition with higher capacity (90 μAh/cm^2) extra lithium was deposited outside of the holes and the initially platted lithium at different directions could merge in the holes (Fig. 2d, S7). There is no significant deformation of the hole structure and no sign of Ti electrode detachment from solid electrolyte, indicating that the 3D structure can not only buffer the large volume expansion during lithium deposition and avoid lithium dendrite growth, but also alleviate internal stress in the solid-state battery and stabilize the interface between electrode and solid electrolyte. For comparison, ASSLMB w/o 3D Ti electrode were investigated. The internal stress generated during lithium plating cannot be well released, leading to the emergence of a large gap between LLZTO and Ti film (Fig. 2e) which may be on account of Ti film being pushed by adjacent deposited lithium stack. Obviously, the generation of those gaps could cause some serious problems such as the weak solid-solid contact and increase of the interface resistance. Moreover, pristine flat Ti layer might even be destroyed by the huge volume expansion (Fig. 2f), and lithium plating became inhomogeneous. As shown in Fig. 2g and 2h, large trunked lithium, which broke the Ti film or even penetrated the solid electrolyte thoroughly, can be observed in a failed cell. For the

purpose of obtaining a deeper understanding of lithium transportation in solid electrolyte and at the interface, a self-designed *in-situ* probing station combining with Scanning Electron Microscope (Fig. S8a) was employed and cell was installed with the lateral side exposed to the field of view (Fig. S8b). The short-circuit process, due to the penetration of the lithium dendrite through the solid electrolyte, was directly observed in a symmetric Li|LLZTO|Li cell. After lithium plating with a low capacity (less than 45μAh/cm^2), cracks generation in the lithium deposited side were first captured, and then the cracks get wider and wider with more lithium deposited (Fig. 2i). On the contrary, no notable changes can be observed at the lithium stripping side (Fig. S9). One possible explanation is that lithium dendrites gradually pierce into the solid electrolyte through gaps between particles which caused by the increase of the stress during the lithium deposition process, thus it can be found in the vicinity of the crack area (Fig. 2j). Noteworthy, it is for the first time that lithium dendrites have been *in-situ* observed. Overall, the solid electrolyte, collector and their interface cannot tolerate the stress induced during lithium plating, and deformation or damage occurs accompanied with lithium dendrite growth. The 3D electrode with holes largely alleviates the interface volume expansion and prevents lithium dendrites from piercing solid electrolyte.

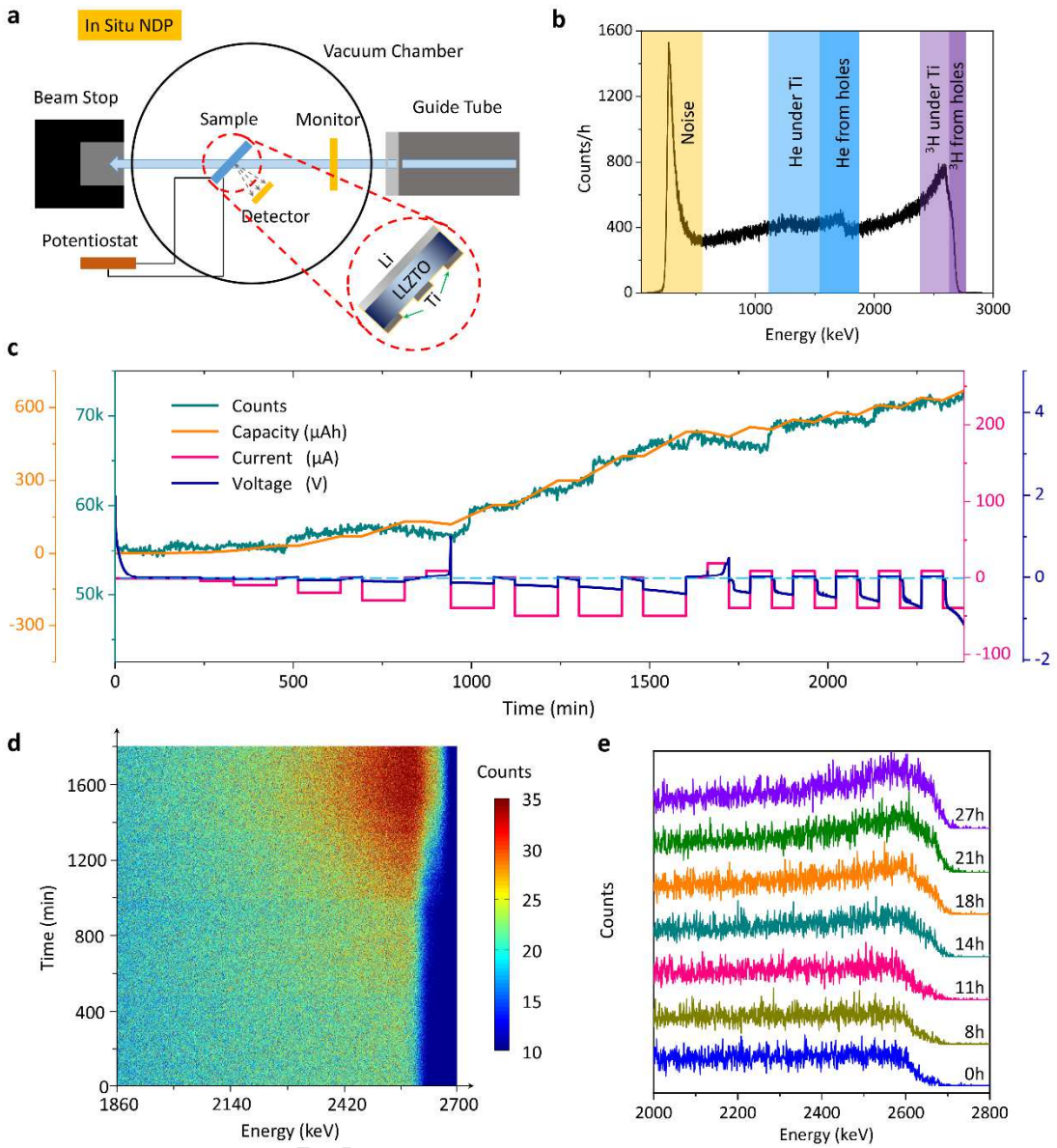

Fig. 3 ***In-situ*** **NDP measurements. (a)** Experimental setup for the *in-situ* NDP measurements. **(b)** A typical NDP spectrum of ASSLMB w/ 3D Ti electrode. **(c)** The voltage (blue), current (red), capacity (orange) and total NDP signal counts (dark cyan) curves recorded during *in-situ* measurement. **(d)** Contour map of *in-situ* NDP spectra collected at 3 min intervals during cycling. **(e)** Integrated curves of NDP data collected in every 1 hour. The curves are stacked along y axis for presentation.

From *ex-situ* and *in-situ* SEM characterizations, difference between initial state and post-discharge state is clearly illustrated while the situation of interface is not yet fully understood on a level of quantitative analysis. However, limited penetrable thickness of various characterization tools restricts the high resolution and *in-situ* direct transmitted observation when electrolyte is totally covered by electrode. Thus, developing more direct characterization means would be complimented for future solid-state lithium metal battery design. Neutron Depth Profile (NDP) as an advanced characterization technique, which highlights a high special resolution along z-axis direction, high sensitivity on light elements, specific quantification and non-destructive measurement properties, may be the ideal tool to study lithium ion interfacial transport behavior in real time. In view of the former understanding that lithium dendrites first appear on the plating side, it's meaningful to measure the interface between Ti film and LLZTO electrolyte. The principle of NDP to detect lithium concentration is that neutron beam enters the vacuum chamber and incidents on the battery contributing to the nuclear reaction between neutrons and ^{6}Li that generates ^{3}H and ^{4}He.

$$^{6}\mathrm{Li} + \mathrm{n} \rightarrow {}^{4}\mathrm{He}\left(2055.51\,\mathrm{keV}\right) + {}^{3}\mathrm{H}(2727.88\,\mathrm{keV})$$

These emitted particles will be collected by a surface barrier detector and analyzed by a multichannel analyzer (Fig. 3a), with which the counts of particles taking different energy are recorded. The linear correspondence for energy calibration between channel number and outgoing particle energy (Table S2, Fig. S11) is adjusted using LiF as calibration sample (Fig. S10) that allows high energy resolution detection.

According to calculation and calibration, by taking the stopping power of PET film into consideration (Fig. S12), several typical sections can be roughly defined (Table S3, Fig. S13). With these parameters, the specific NDP spectrum of ASSLMB w/ 3D Ti electrode could be analyzed (Fig. 3b). The low energy section in yellow is regarded as background noise. And with the increase of energy the sections of ^{4}He and ^{3}H, which are in blue and purple respectively, are sorted out. The total energy uncertainty includes three parts of detector resolution, geometry effects and energy straggling. The first two parts which is related to the instrument itself can be determined by the thin standard samples. The third part related to scattering process can be computed by using the Monte Carlo TRIM code of the SRIM package (Fig. S14). Furthermore, the kinetic energy of the emergent particles traveling through Ti layer attenuates is much more than those through etched holes, thus the ^{4}He and ^{3}H can be further divided into the 'under Ti' part and the 'from hole' part. The wonder of whether the counts of ^{4}He and ^{3}H in certain scales can reliably reflect the lithium amount turns out. Adding the counts of specific sections together to compare with the battery charge capacity should be a reliable demonstration to that problem. In order to get the quantitative interface evolution, the battery was charged under different current density (Fig. 3c), which gradually increased could improve interface invasive and the *in-situ* measure of NDP underwent every 3 minutes depending on the instrument's time resolution. After about 2460 minutes, the measured lithium capacity displays great consistency with the sum of counts. It is surprising that even the discharge capacity is far more than the hole could host, the cell still charge/discharge normally without short circuit (Fig.

S15), as a comparison, the micro-short circuit appears early at about 180 min in ASSLMB w/o 3D Ti electrode (Fig. S19a). Meanwhile, the ASSLMB undergo the impedance decreasing process owing to the deposited lithium piercing Ti or gathering in the void space. In Fig. 3e, the counts of ^{3}H increase by time, and each different energy range corresponds to different materials depth, as a result, 2560-2630 keV shows the most dramatic changes which means lithium plates the most in the void space (Fig. S16) plus the peak of the curve changes in shape slightly at around 2595 keV. The peak's change much more directly exhibits in Fig. 3d that when time increases, the vertical margin at 2595 keV extends out and the number of counts grows fast, which projects the growth of lithium in the void space. In addition, Fig. S17 is a larger scale version of Fig. 3d that displays four visible variable counts lines at around 1350, 1760, 2550, 2620 keV manifesting lithium plating both in void space and under the Ti film. Because the closer lithium is to the surface, the higher the resultant particle energy will be, and the more counts will be detected as well. Therefore, we can conclude that the 3D structure with void space on Ti can doubtlessly conduct the lithium to plate and grow in the void space, and it can be inferred that this buffer mechanism should help solving the volume change problem at the interface. To have a precious understanding of the lithium plating behavior, more NDP data is utilized to get a clearer picture.

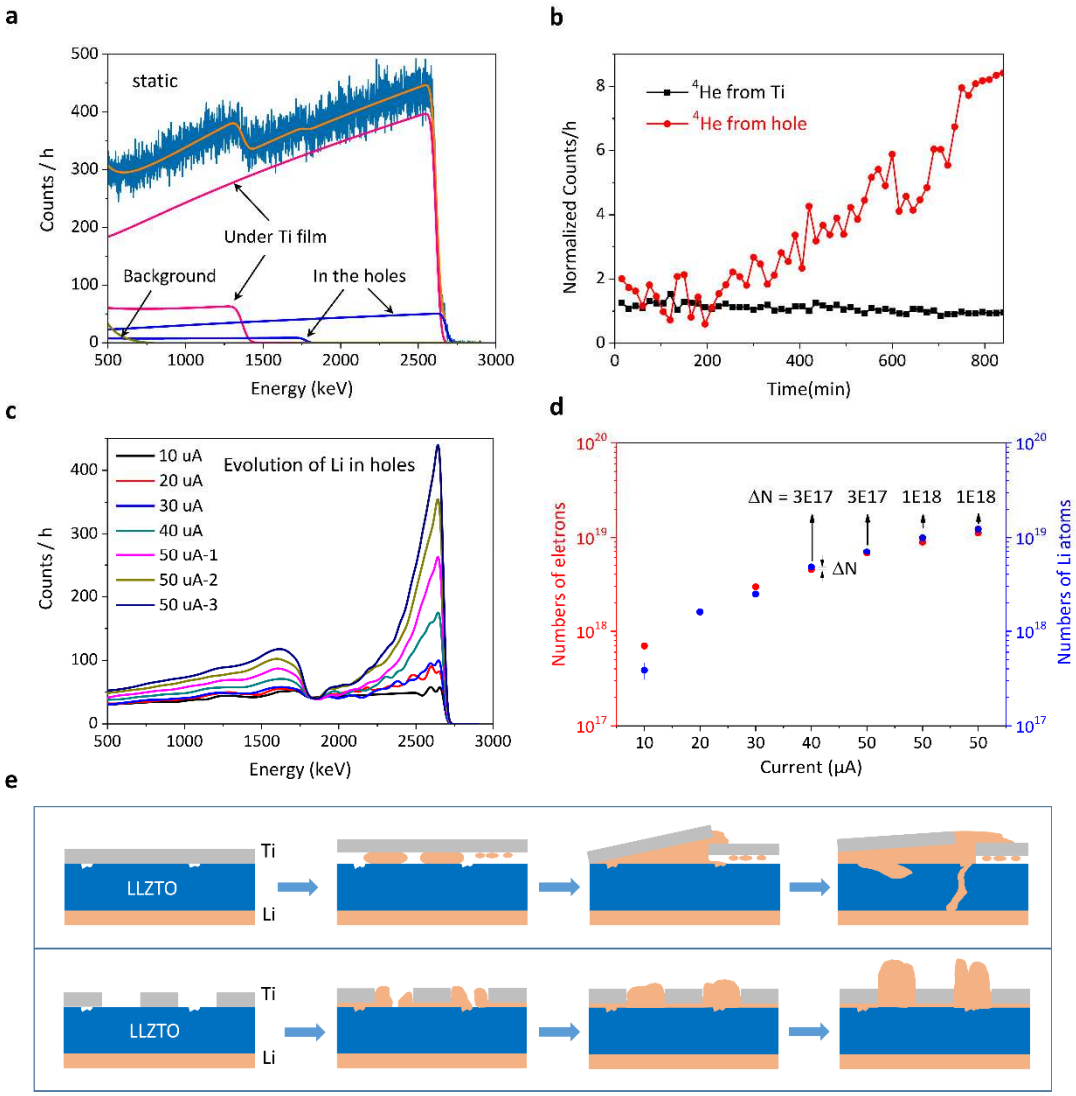

Fig. 4 NDP spectra analysis and lithium plating modeling. (a) NDP spectrum unfolding. **(b)** Lithium plating ratio under Ti film and in the hole over time reflected by ^{4}He signal. **(c)** Total signals of ^{3}H and ^{4}He from the holes gives the evolution of lithium plating in the holes. **(d)** The differences between the numbers of electrons and lithium atoms at different discharged conditions. **(e)** Schematic illustration of lithium plating under Ti film with and without holes.

Through simulation and calculation by spectrum unfolding, the data of static state and

signals from different sources can be separated. The simulation results and the lithium distribution of the solid-state test battery match well (Fig. 4a). After discharging under different current density sequentially, both ^{3}H and ^{4}He have shown remarkable increase in peak area, which relate to the increase in the lithium abundance near the surface. Moreover, the stopping power of ^{4}He at Ti film is large enough to distinguish between the increasing lithium atoms under Ti film and in the holes. In order to quantitatively understand the accurate proportion of lithium from under Ti and from holes over time, the counts of ^{4}He and ^{3}H from under Ti of the static state are used to normalize the *in-situ* counts data from different sources. The existence of 'hole' structure is contributing to the fact that only a small amount of lithium deposits under Ti film at the beginning of the discharge process, whereas almost all the lithium from anode accumulates into the holes while the under Ti part keeps still (Fig. 4b). And the error analysis of ^{4}He signals emitting from holes and below Ti film manifest the reliability of the data (Fig. S18). By comparison, an obvious signal of lithium breaking through Ti film which could be clearly testified by the first derivation curve of normalized counts (Fig. S19d) is captured after lithium plating in solid-state battery with flat Ti film (Fig. S19b, c). Due to the lithium increment under the Ti film is below the NDP detection limits, the NDP spectrum in the holes can be fitted by the ideal model (Fig.4c). Meanwhile, after concentration calibration of the static battery sample, the increment of lithium atoms in the holes at different discharging conditions is proportional to the increasing counts in corresponding spectrum. It's worth noting that the number of electrons passing through the outer circuit is in great agreement

with the number of lithium atoms in the holes (Fig.4d). Therefore, there comes out the possible model of lithium plating in the normal flat and with-hole battery system (Fig. 4e). In normal solid-state batteries, huge volume change during discharge may cause the swell of collector. In addition, the inner stress at the interface may lead lithium dendrites to grow into the inside of solid electrolyte along the particles' interval, which presents in the same form of crack propagation and creeping in symmetric Li|LLZTO|Li cell. On the contrary, in the modified one, during discharge, only a little lithium will deposit under Ti film and contact with electrolyte at initial discharging stage, thereafter the majority lithium will congregate in the void space which significantly reduce the volume change at the interface, prevent dendrite penetration and promote the cycle stability.

In conclusion, lithium plating at the interface between solid electrolyte and electrode will inevitably cause mechanical problems that inhibit the stable cycling of the solid-state batteries. In this work, we for the first time directly observed the crack propagation accompanied with lithium dendrite growth at the micro-scale in real time in the symmetric Li|LLZTO|Li cell. The destroy of solid electrolyte/electrode interface, due to the huge volume expansion as well as the lithium dendrite growth, has also been observed in solid-state lithium metal battery with flat Ti film electrode as current collector. It is naturally to expect that the electrode with 3D porous structure framework can accommodate lithium storage without incurring volume expansion, and we did confirm that the majority of lithium congregated in the void

space of a well-designed solid-state battery with patterned Ti electrode. However, we found that lithium preferred to deposit at the interface between solid electrolyte and Ti electrode at the initial stage of plating, leading to the unstable interface properties and degradation of the battery performances. As a result, the structured electrode is necessary for relieving the huge volume expansion, releasing the stress at the interface and preventing lithium dendrites from penetration. But the rare interfacial lithium plating can still not satisfy the demands for solid-state battery application. A perfect design of solid-state battery interface might need to combine a 3D framework structure to accommodate lithium storage and a gradient or selective interfacial electronic conductivity to guide the lithium plating into the void space in the 3D structure instead of the interface.

Methods & Materials

Fabrication of patterned Ti electrode on LLZTO solid electrolyte pellet

The fabrication of patterned Ti electrode on LLZTO solid electrolyte pellet was achieved by a series of micro-fabrication processes including electron beam evaporation (FU-12PEB, F.S.E CORPORATION), photolithography (MA6, Karl Süss GmbH) and ion beam etching (LKJ-1D-150, Beijing Institute of Advanced Ion Beam Technology). The garnet LLZTO ($Li_7La_3Zr_2Ta_{0.6}O_{12}$) solid electrolyte pellet was obtained from Xiangxin Guo's group (1mm in thickness) [50], was firstly polished to obtain a clean and smooth surface that can meet the requirement for the NDP measurement. And then Ti film was deposited on the polished LLZTO surface

using the electron beam evaporation system and the thickness was controlled to around 1 μm. In order to prevent the LLZTO ceramic pellet from contacting the water in developer during photoresist developing process, the bare LLZTO side was tightly pasted on a Si wafer using a positive photoresist (AZ6130). After pre-baking (180℃, 10 min), adhesion primer vapor treatment (HMDS, 180℃, 10min), photoresist spin-coating (AZ6130, 4000 r/min), soft baking (110℃, 1min), photolithography (8s, 11mJ/cm^2) and development (1min), the sample were transferred to the chamber of an ion beam etching system (periodic etching with 3min interval, 5℃, 50 mJ/cm^2). Similar procedures were performed on a Si wafer which was used to calibrate the etching rate. It's rather remarkable that the total etching depth cannot be monitored in real time, so the accompanying Si wafer should be taken out in the middle of the etching process to calibrate the real etching rate, to make sure that the Ti film has been etched completely (exposure of LLZTO). After etching, the ceramic pellet was transferred to a microwave plasma photoresist ashing system (PS 210, PVA TePla America, Inc.) to remove the photoresist. At last, the fabricated ceramic pellet with patterned Ti electrode was transferred into glovebox to construct the *in-situ* cell.

NDP Measurement

The open surface Li-ion battery specimen, undergoing several charging/discharging cycles (Fig. 3c), were analyzed by the *in-situ* neutron depth profiling (NDP) instrument at the Center for Neutron Research (NCNR) of the National Institute of Standards and Technology (NIST). The *in-situ* NDP experimental setup is

schematically illustrated in Fig. 3a. The cold neutron beam (< 4 meV) with a flux of 10^9 cm^{-2} s^{-1} entered the chamber via a thin aluminum window and passed through the charging/discharging battery specimen controlled by a potentiometer. The isotope ^6Li in the battery specimen underwent a nuclear reaction (as shown in Equation) when absorbing neutrons results in two highly energetic charged particles (alpha and triton particles) emission. After interacting with the other electrons and nuclei in the battery specimen, the charged particles from LLZTO layer lost their energy and exited the battery specimen. Nevertheless, these particles would not lose its energy after emerging from the battery specimen surface, because the NDP instrument was housed in a vacuum chamber. Finally, each charged particle energy spectrum was recorded during a period of 3 min by surface barrier detector. By detecting the residual energy of these charged particles, the original position of the neutron absorption, i.e. the depth of isotope ^6Li, can be determined using the material's stopping power. It is noted that NDP technique mimics the behavior of all Li atoms, even though it is only sensitive to isotope ^6Li which is about 7.5% in natural lithium. For the depth resolution (z-axis orientation), it is determined by the energy resolution of the detector, the geometry effects and the energy straggling. So the resolution of ^4He and ^3H is different for their different stopping power. By calculating, the depth resolution of the system in this study is about 140 nm for tritium particles, and about 30 nm for α particles.

Operando SEM Measurement

Li|LLZTO|Li symmetric solid state battery was assembled in glovebox by cold pressing lithium foil on the LLZTO electrolyte pellet. Then the intact ceramic plate was vertically cut to expose its cross-section for operando SEM observation. The self-designed *in-situ* probing station (Fig. S8a-b), which can be installed in Scanning Electron Microscope, contains two metal probes that are controlled by micro-motor for minor movement in three directions. The solid state battery was fixed vertically on the platform, charging/discharging through the two probes connecting to LAND. SEM images with high resolution were captured about every 1 min during the charge and discharge process.

Acknowledgements

This work was supported by National Key R&D Program of China (Grants No. 2016YFB0100100), National Natural Science Foundation of China (Grants No. 51822211), the Foundation for Innovative Research Groups of the National Natural Science Foundation of China (grant no. 51421002), Science and technology planning project of Guangdong Province (grant no. 2017B090921001) and State Grid Technology project (Study on the mechanism and characterization of lithium dendrite growth in lithium ion batteries, Grants No. DG71-17-010).

References

[1] M. Armand, J.M. Tarascon, Building better batteries, Nature 451 (2008) 652-657.

[2] Y.M. Chiang, Building a Better Battery, Science 330 (2010) 1485-1486.

[3] J.M. Tarascon, M. Armand, Issues and challenges facing rechargeable lithium batteries, Nature 414 (2001) 359-367.

[4] K. Xu, Nonaqueous liquid electrolytes for lithium-based rechargeable batteries, Chem. Rev. 104 (2004) 4303-4417.

[5] K. Xu, Electrolytes and interphases in Li-ion batteries and beyond, Chem. Rev. 114 (2014) 11503-11618.

[6] F. Ding, W. Xu, X. Chen, J. Zhang, M.H. Engelhard, Y. Zhang, B.R. Johnson, J.V. Crum, T.A. Blake, X. Liu, J.-G. Zhang, Effects of carbonate solvents and lithium salts on morphology and coulombic efficiency of lithium electrode, J. Electrochem. Soc. 160 (2013) A1894-A1901.

[7] F. Ding, W. Xu, G.L. Graff, J. Zhang, M.L. Sushko, X. Chen, Y. Shao, M.H. Engelhard, Z. Nie, J. Xiao, X. Liu, P.V. Sushko, J. Liu, J.-G. Zhang, Dendrite-free lithium deposition via self-healing electrostatic shield mechanism, J. Am. Chem. Soc. 135 (2013) 4450-4456.

[8] Y. Zhang, J. Qian, W. Xu, S.M. Russell, X. Chen, E. Nasybulin, P. Bhattacharya, M.H. Engelhard, D. Mei, R. Cao, F. Ding, A.V. Cresce, K. Xu, J.-G. Zhang, Dendrite-free lithium deposition with self-aligned nanorod structure, Nano Lett. 14 (2014) 6889-6896.

[9] J.M. Zheng, M.H. Engelhard, D.H. Mei, S.H. Jiao, B.J. Polzin, J.G. Zhang, W. Xu, Electrolyte additive enabled fast charging and stable cycling lithium metal batteries, Nat. Energy 2 (2017) 17012.

[10] S.H. Jiao, X.D. Ren, R.G. Cao, M.H. Engelhard, Y.Z. Liu, D.H. Hu, D.H. Mei,

J.M. Zheng, W.G. Zhao, Q.Y. Li, N. Liu, B.D. Adams, C. Ma, J. Liu, J.G. Zhang, W. Xu, Stable cycling of high-voltage lithium metal batteries in ether electrolytes, Nat. Energy 3 (2018) 739-746.

[11] N. Kamaya, K. Homma, Y. Yamakawa, M. Hirayama, R. Kanno, M. Yonemura, T. Kamiyama, Y. Kato, S. Hama, K. Kawamoto, A. Mitsui, A lithium superionic conductor, Nat. Mater. 10 (2011) 682-686.

[12] Y. Kato, S. Hori, T. Saito, K. Suzuki, M. Hirayama, A. Mitsui, M. Yonemura, H. Iba, R. Kanno, High-power all-solid-state batteries using sulfide superionic conductors, Nat. Energy 1 (2016) 16030.

[13] W. Zhou, S. Wang, Y. Li, S. Xin, A. Manthiram, J.B. Goodenough, Plating a dendrite-free lithium anode with a polymer/ceramic/polymer sandwich electrolyte, J. Am. Chem. Soc. 138 (2016) 9385-9388.

[14] A. Manthiram, X. Yu, S. Wang, Lithium battery chemistries enabled by solid-state electrolytes, Nat. Rev. Mater. 2 (2017) 16103.

[15] W. Xu, J. Wang, F. Ding, X. Chen, E. Nasybulin, Y. Zhang, J.-G. Zhang, Lithium metal anodes for rechargeable batteries, Energy Environ. Sci. 7 (2014) 513-537.

[16] M.D. Tikekar, S. Choudhury, Z.Y. Tu, L.A. Archer, Design principles for electrolytes and interfaces for stable lithium-metal batteries, Nat. Energy 1 (2016) 1-7.

[17] X.B. Cheng, R. Zhang, C.Z. Zhao, Q. Zhang, Toward safe lithium metal anode in rechargeable batteries: A review, Chem. Rev. 117 (2017) 10403-10473.

[18] D.C. Lin, Y.Y. Liu, Y. Cui, Reviving the lithium metal anode for high-energy batteries, Nat. Nanotechnol. 12 (2017) 194-206.

[19] P. Albertus, S. Babinec, S. Litzelman, A. Newman, Status and challenges in enabling the lithium metal electrode for high-energy and low-cost rechargeable batteries, Nat. Energy 3 (2018) 16-21.

[20] Y.Y. Ren, Y. Shen, Y.H. Lin, C.W. Nan, Direct observation of lithium dendrites inside garnet-type lithium-ion solid electrolyte, Electrochem. Commun. 57 (2015) 27-30.

[21] F. Aguesse, W. Manalastas, L. Buannic, J.M.L. del Amo, G. Singh, A. Llordes, J. Kilner, Investigating the dendritic growth during full cell cycling of garnet electrolyte in direct contact with Li metal, ACS Appl. Mater. Interfaces 9 (2017) 3808-3816.

[22] E.J. Cheng, A. Sharafi, J. Sakamoto, Intergranular Li metal propagation through polycrystalline $Li_{6.25}Al_{0.25}La_3Zr_2O_{12}$ ceramic electrolyte, Electrochim. Acta 223 (2017) 85-91.

[23] L. Porz, T. Swamy, B.W. Sheldon, D. Rettenwander, T. Frömling, H.L. Thaman, S. Berendts, R. Uecker, W.C. Carter, Y.-M. Chiang, Mechanism of lithium metal penetration through inorganic solid electrolytes, Adv. Energy Mater. (2017) 1701003.

[24] F. Han, A.S. Westover, J. Yue, X. Fan, F. Wang, M. Chi, D.N. Leonard, N.J. Dudney, H. Wang, C. Wang, High electronic conductivity as the origin of lithium dendrite formation within solid electrolytes, Nat. Energy 4 (2019) 187-196.

[25] Y. Iriyama, T. Kako, C. Yada, T. Abe, Z. Ogumi, Charge transfer reaction at the lithium phosphorus oxynitride glass electrolyte/lithium cobalt oxide thin film interface, Solid State Ion. 176 (2005) 2371-2376.

[26] K. Park, B.-C. Yu, J.-W. Jung, Y. Li, W. Zhou, H. Gao, S. Son, J.B. Goodenough,

On the electrochemical nature of the cathode interface for a solid-state lithium-ion battery: Interface between $LiCoO_2$ and garnet-$Li_7La_3Zr_2O_{12}$, Chem. Mat. 28 (2016) 8051-8059.

[27] A. Mauger, M. Armand, C.M. Julien, K. Zaghib, Challenges and issues facing lithium metal for solid-state rechargeable batteries, J. Power Sources 353 (2017) 333-342.

[28] X.S. Yin, W. Tang, I.D. Jung, K.C. Phua, S. Adams, S.W. Lee, G.W. Zheng, Insights into morphological evolution and cycling behaviour of lithium metal anode under mechanical pressure, Nano Energy 50 (2018) 659-664.

[29] X. Han, Y. Gong, K. Fu, X. He, G.T. Hitz, J. Dai, A. Pearse, B. Liu, H. Wang, G. Rublo, Y. Mo, V. Thangadurai, E.D. Wachsman, L. Hu, Negating interfacial impedance in garnet-based solid-state Li metal batteries, Nat. Mater. 16 (2017) 572-579.

[30] B. Liu, K. Fu, Y. Gong, C. Yang, Y. Yao, Y. Wang, C. Wang, Y. Kuang, G. Pastel, H. Xie, E.D. Wachsman, L. Hu, Rapid thermal annealing of cathode-garnet interface toward high-temperature solid state batteries, Nano lett. 17 (2017) 4917-4923.

[31] W. Luo, Y.H. Gong, Y.Z. Zhu, Y.J. Li, Y.G. Yao, Y. Zhang, K. Fu, G. Pastel, C.F. Lin, Y.F. Mo, E.D. Wachsman, L.B. Hu, Reducing interfacial resistance between garnet-structured solid-state electrolyte and Li-metal anode by a germanium layer, Adv. Mater. 29 (2017) 1606042.

[32] A. Sharafi, E. Kazyak, A.L. Davis, S.H. Yu, T. Thompson, D.J. Siegel, N.P. Dasgupta, J. Sakamoto, Surface chemistry mechanism of ultra-low interfacial

resistance in the solid-state electrolyte $Li_7La_3Zr_2O_{12}$, Chem. Mat. 29 (2017) 7961-7968.

[33] H. Xu, Y. Li, A. Zhou, N. Wu, S. Xin, Z. Li, J.B. Goodenough, Li_3N-modified garnet electrolyte for all-solid-state lithium metal batteries operated at 40 °C, Nano lett. 18 (2018) 7414-7418.

[34] R.C. Xu, F.D. Han, X. Ji, X.L. Fan, J.P. Tu, C.S. Wang, Interface engineering of sulfide electrolytes for all-solid-state lithium batteries, Nano Energy 53 (2018) 958-966.

[35] R. Sudo, Y. Nakata, K. Ishiguro, M. Matsui, A. Hirano, Y. Takeda, O. Yamamoto, N. Imanishi, Interface behavior between garnet-type lithium-conducting solid electrolyte and lithium, metal, Solid State Ion. 262 (2014) 151-154.

[36] Z. Liu, Y. Qi, Y.X. Lin, L. Chen, P. Lu, L.Q. Chen, Interfacial study on solid electrolyte interphase at Li metal anode: Implication for Li dendrite growth, J. Electrochem. Soc. 163 (2016) A592-A598.

[37] C.L. Tsai, V. Roddatis, C.V. Chandran, Q.L. Ma, S. Uhlenbruck, M. Bram, P. Heitjans, O. Guillon, $Li_7La_3Zr_2O_{12}$ interface modification for Li dendrite prevention, ACS Appl. Mater. Interfaces 8 (2016) 10617-10626.

[38] K. Kerman, A. Luntz, V. Viswanathan, Y.M. Chiang, Z.B. Chen, Review-Practical challenges hindering the development of solid state Li ion batteries, J. Electrochem. Soc. 164 (2017) A1731-A1744.

[39] L. Cheng, W. Chen, M. Kunz, K. Persson, N. Tamura, G.Y. Chen, M. Doeff, Effect of surface microstructure on electrochemical performance of garnet solid

electrolytes, ACS Appl. Mater. Interfaces 7 (2015) 2073-2081.

[40] K. Fu, Y.H. Gong, J.Q. Dai, A. Gong, X.G. Han, Y.G. Yao, C.W. Wang, Y.B. Wang, Y.N. Chen, C.Y. Yan, Y.J. Li, E.D. Wachsman, L.B. Hu, Flexible, solid-state, ion-conducting membrane with 3D garnet nanofiber networks for lithium batteries, Proc. Natl. Acad. Sci. U. S. A. 113 (2016) 7094-7099.

[41] X. Tao, Y. Liu, W. Liu, G. Zhou, J. Zhao, D. Lin, C. Zu, O. Sheng, W. Zhang, H.-W. Lee, Y. Cui, Solid-state lithium–sulfur batteries operated at 37 °C with composites of nanostructured $Li_7La_3Zr_2O_{12}$/carbon foam and polymer, Nano lett. 17 (2017) 2967-2972.

[42] C.W. Wang, Y.H. Gong, B.Y. Liu, K. Fu, Y.G. Yao, E. Hitz, Y.J. Li, J.Q. Dai, S.M. Xu, W. Luo, E.D. Wachsman, L.B. Hu, Conformal, nanoscale ZnO surface modification of garnet-based solid-state electrolyte for lithium metal anodes, Nano lett. 17 (2017) 565-571.

[43] S.M. Xu, D.W. McOwen, C.W. Wang, L. Zhang, W. Luo, C.J. Chen, Y.J. Li, Y.H. Gong, J.Q. Dai, Y.D. Kuang, C.P. Yang, T.R. Hamann, E.D. Wachsman, L.B. Hu, Three-dimensional, solid-state mixed electron-ion conductive framework for lithium metal anode, Nano lett. 18 (2018) 3926-3933.

[44] Q. Zhang, H.L. Wan, G.Z. Liu, Z.G. Ding, J.P. Mwizerwa, X.Y. Yao, Rational design of multi-channel continuous electronic/ionic conductive networks for room temperature vanadium tetrasulfide-based all-solid-state lithium-sulfur batteries, Nano Energy 57 (2019) 771-782.

[45] S.C. Nagpure, R.G. Downing, B. Bhushan, S.S. Babu, L. Cao, Neutron depth

profiling technique for studying aging in Li-ion batteries, Electrochim. Acta 56 (2011) 4735-4743.

[46] X. Zhang, T.W. Verhallen, F. Labohm, M. Wagemaker, Direct Observation of Li-ion transport in electrodes under nonequilibrium conditions using neutron depth profiling, Adv. Energy Mater. 5 (2015) 1500498.

[47] C.W. Wang, Y.H. Gong, J.Q. Dai, L. Zhang, H. Xie, G. Pastel, B.Y. Liu, E. Wachsman, H. Wang, L.B. Hu, In situ neutron depth profiling of lithium metal-garnet interfaces for solid state batteries, J. Am. Chem. Soc. 139 (2017) 14257-14264.

[48] S.S. Lv, T. Verhallen, A. Vasileiadis, F. Ooms, Y.L. Xu, Z.L. Li, Z.C. Li, M. Wagemaker, Operando monitoring the lithium spatial distribution of lithium metal anodes, Nat. Commun. 9 (2018) 2152.

[49] J.F.M. Oudenhoven, F. Labohm, M. Mulder, R.A.H. Niessen, F.M. Mulder, P.H.L. Notten, In situ neutron depth profiling: A powerful method to probe lithium transport in micro-batteries, Adv. Mater. 23 (2011) 4103–4106.

[50] C. Chen, Q. Li, Y.Q. Li, Z.H. Cui, X.X. Guo, H. Li, Sustainable interfaces between Si anodes and garnet electrolytes for room-temperature solid-state batteries, ACS Appl. Mater. Interfaces 10 (2018) 2185-2190.

Highlights:

(1) Lithium plating was directly observed in all-solid-state battery by *in-situ* neutron depth profile method.

(2) The lithium perfers to plate at the void space of the 3D electrode.

(3) The 3D electrode with void space enables revesible lithium plating/stripping without dendrite growth.